Available online at www.sciencedirect.com
ScienceDirect
Solar Energy 84 (2010) 1526–1537
SOLAR ENERGY
www.elsevier.com/locate/solener

Using CAD software to simulate PV energy yield – The case of product integrated photovoltaic operated under indoor solar irradiation

N.H. Reich [a,*], W.G.J.H.M. van Sark [a], W.C. Turkenburg [a], W.C. Sinke [a,b]

[a] Dept. of Science, Technology and Society, Copernicus Institute for Sustainable Development and Innovation, Utrecht University, Heidelberglaan 2, 3584 CS, Utrecht, The Netherlands
[b] Energy Research Centre of the Netherlands (ECN), Petten, The Netherlands

Received 27 February 2009; received in revised form 17 May 2010; accepted 18 May 2010
Available online 18 June 2010

Communicated by: Associate Editor Nicola Romeo

Abstract

In this paper, we show that photovoltaic (PV) energy yields can be simulated using standard rendering and ray-tracing features of Computer Aided Design (CAD) software. To this end, three-dimensional (3-D) sceneries are ray-traced in CAD. The PV power output is then modeled by translating irradiance intensity data of rendered images back into numerical data. To ensure accurate results, the solar irradiation data used as input is compared to numerical data obtained from rendered images, showing excellent agreement. As expected, also ray-tracing precision in the CAD software proves to be very high. To demonstrate PV energy yield simulations using this innovative concept, solar radiation time course data of a few days was modeled in 3-D to simulate distributions of irradiance incident on flat, single- and double-bend shapes and a PV powered computer mouse located on a window sill. Comparisons of measured to simulated PV output of the mouse show that also in practice, simulation accuracies can be very high. Theoretically, this concept has great potential, as it can be adapted to suit a wide range of solar energy applications, such as sun-tracking and concentrator systems, Building Integrated PV (BIPV) or Product Integrated PV (PIPV). However, graphical user interfaces of 'CAD-PV' software tools are not yet available.

Keywords: CAD; PV; Ray-tracing; Simulation; Performance; PIPV; BIPV

1. Introduction

Currently, the time needed for energy balance assessments of Product Integrated PV (PIPV) systems is substantial, because computer software to simulate the energy yield of solar cells incorporated into these PIPV systems does not yet exist. Calculating PV power output at a given irradiance intensity and spectral composition is not easy, and variations in product design as well as the variety of possible PV configurations (solar cell type, interconnection, etc.) further increases complexity. Energy yield assessments are also hampered by a broad range of end-user behaviour, implying large uncertainty in calculated results. Moreover, many PIPV appliances are designed for indoor use. Daylight availability in the indoor environment, however, is a complex matter in itself. In addition, PV gadgets can be energized by room lighting. The spectral composition of artificial light can differ considerably from daylight that is filtered by window glazing. Moreover, difficulties arise when considering that wavelength' above 780 nm are not covered in terms of illuminance (Lux) levels, which, however, are frequently used in daylight related tasks, but which cannot be used directly to estimate a PV energy yield.

In this study, we aim to address and alleviate some of these problems by employing Computer Aided Design (CAD) software to simulate the energy yield of PIPV systems.

* Corresponding author.
E-mail address: N.H.Reich@uu.nl (N.H. Reich).

0038-092X/$ - see front matter © 2010 Elsevier Ltd. All rights reserved.
doi:10.1016/j.solener.2010.05.015

This approach is innovative, although CAD software and embedded rendering functionality itself is already established. Consequently, the presented approach is not demanding on product designers, as proficiency in yet another software tool is not required. Nevertheless, the versatility of the simulation approach is considerable: almost any number and type of 3D-shapes can easily be created or altered virtually within any CAD software that allows image rendering. To ensure the simulation of irradiation is performed on a physically sound basis, we use CAD ray-tracing for the rendering, which relies on physical properties of light-rays and photons, respectively.

Already in 1994, ray-tracing software was used for PV energy yield prediction purposes. Here, RADIANCE (Larson et al., 1998) was used by Kovach (1994) to study the effects of inhomogeneous irradiation distributions on the output of PV arrays in an urban environment. During the design process of a PV powered wireless computer mouse (Reich, 2006; Reich et al., 2007, 2009), however, we found that using CAD-rendered images did not permit straightforward PV energy yield predictions. Reinders (2007) demonstrated, by a tool named '3D-PV', how CAD software can be used to assess variations of irradiation distributions incident onto PV areas by means of the 'ambient occlusion' rendering technique. The '3D-PV' tool allowed to evaluate shading effects caused by a PV product's own geometry, however, not to simulate PV power output and neither modeling options of irradiation were included.

In this article, we aim to demonstrate how ray-tracing and rendering features of CAD software can be used to simulate PV energy yields with any spatial distribution of irradiance in any three-dimensional (3-D) CAD scenery. In preliminary evaluations we already demonstrated the feasibility of this simulation concept (Reich et al., 2008, 2009). In this paper, we also focus on the precision with which ray-tracing in CAD can be performed and address the overall simulation accuracy too. To this end, actually measured data of PV energy yield is compared with the one simulated using the 'CAD-PV' simulation concept.

Despite the envisaged broad applicability of the presented simulation approach in other fields of PV appliances, such as for energy yield simulation of PV-modules operated outdoors, we focus on PIPV in particular, due to the research framework of this study (Alsema et al., 2005). Detailed descriptions of PIPV related aspects have already been given elsewhere (Reich et al., 2009; Roth, 2008). In addition, the focus in this study is on the south-facing window sill location. For one, users may place their PIPV system on a window sill for the purpose of "sunbathing" (Reich et al., 2009). Furthermore, simulating irradiation conditions and energy yields of PV at a window sill is near impossible using conventional methods (Nieuwenhout et al., 2007; Wagemann and Estrich, 1994), despite the high reduction of complexity regarding PIPV systems by choosing this location.

2. Methodology

2.1. General approach

The concept of the presented simulation approach is to generate a 3-D solid-angle distribution of irradiance and to add this to a 3-D scene with 3-D product geometries. Subsequently, the scene is rendered. As CAD software we use, in this study, the 3D Studio Max (3ds Max) program from AutoDesk, because preliminary evaluations of the concept (Reich et al., 2008) lead to readily available script code ('MAXSCRIPT'). The solid-angle irradiance distribution can be represented by a finite number of directional light sources in 3ds Max, by arranging light sources equidistantly across a hemisphere. This approach is used instead of relying on the 3ds Max incorporated daylight simulation features, to keep control on what actually is simulated as the 3-D solar energy distribution. Here, only a single light source is considered as direct-beam intensity, with adjusted intensity and position of the CAD light according to beam intensity and position of the sun. Solid-angle distributions of irradiance are derived according to the model of Perez et al. (1987) and sun position algorithms (Grena, 2008).

2.2. Converting rendered images into numerical data

Rendered 'photorealistic' images only contain the fraction of light reflected into the specific view-perspective, because only this fraction reflected by a particular surface is seen by the human eye. The irradiance intensity incident onto a surface of the rendered geometries, however, therefore needs to be computed by the rendering engine as well, in order to let it compute the fraction reflected into a specific direction. Theoretically, the intensity incident onto a given surface can therefore also be retrieved for any rendering engine. In 3ds Max, the irradiance intensity that is incident onto a modeled geometry (i.e., not only the reflected fraction) can be retrieved in the form of either colored bitmap images or by grey-scale images. We opted to use RGB instead of grey-scales during the early stages of software development. The intensity (I) incident onto a particular spot (pixel) of the geometry needs to be decoded from the RGB-encoded values into numerical data, at each pixel of the rendered image, to be processed further (e.g. to calculate a PV power output under 'rendered irradiance intensity' that is simulated to be incident onto a particular spot of the geometry). For the RGB scale used by 3ds Max we derived the following equation to translate RGB-encoded data into numerical data of irradiance intensity. The photocurrent density (J_{Ph}) induced in the solar cell can be calculated accordingly.

$$I = I_0 \cdot \frac{(1 - B + G + 3R - 2RG)}{4} \tag{1}$$

$$J_{Ph} = J_{Ph,0} \cdot \frac{(1 - B + G + 3R - 2RG)}{4} \tag{2}$$

in which the maximum light intensity I_0 (W/m^2) and the maximum light generated current density $J_{Ph,0}$ (A/m^2) are associated to the upper end of the RGB-scale and R, G, and B are the normalized red, green, and blue values of the RGB-encoded rendering, ranging from zero to unity in Eq. (1). This equation is related to the particular scale used by 3ds Max, in which the color ranges from blue (B) over green (G), to red (R), and was derived graphically once the RGB value pairs that result in the specific color scale have been determined (see Fig. 1 and description in caption).

2.3. Theoretical validation

As a new method is presented, some results of the validations made throughout the development process are provided. A critical point in the beginning was to ensure that the super-position of light is handled accurately, as this is a prerequisite for the entire simulation approach. Since this proved to be the case, the first validation conducted was to vary the incident angle of the light beam emitted from a single light source, to test whether the cosine dependence of light intensity as a function of incident angle holds. To this end, the incident angle of a CAD light source with respect to a simple plane geometry, modeled in the CAD scenery, was varied. Next, a transparent plane was introduced into the light path (Fig. 2a) as this allows to also address ray-tracing performance of the 3ds Max embedded ray-tracer regarding light transmittance (MentalRay). The transmittance determined by 3ds Max was compared with transmittance calculated by Fresnel equations and Snell's law, incorporated into a simple spreadsheet model. Finally, we tested the accuracy with which reflections are ray-traced with MentalRay in 3ds Max. Here, we considered two parallel planes, into which a light beam is sent. The intensity of this beam is attenuated dependent on defined reflectivity of the two parallel boxes, between which the light beam bounces back and forth (see Fig. 2b).

For the 3ds Max and ray-tracer specific settings, we tested all three available rendering choices, namely Global Illumination (GI) and 'caustic' forward ray-tracing as well as Final Gathering (FG) backward ray-tracing. Transparencies for the material settings were modeled with disabled translucency and reflectivity by defining zero transparency. For all materials, unity glossiness factors as well as zero-roughness coefficients were used (Murdock, 2009).

2.4. Indoor sceneries, irradiation data and experimental setup

Two indoor sceneries of window sill locations have been modeled. In a first approach, a simplified indoor scenery was created by only defining a single plane, which represents the window glazing, and assigning a transparency-property to this plane (transmittance set to a rather low 80% and reflectance set to 'Index Of Refraction (IOR) 1.52). The necessity of modeling the walls of the interior was avoided by only including light sources below 90° and above 270° azimuth angle. Three relatively simple 3-D shapes were chosen to be modeled in this simplified scenery, as this is sufficient to illustrate ray-tracing and rendering features of CAD and to evaluate its applicability for PV energy yield predictions. The scenery and considered 3-D shapes are illustrated in Fig 3. As 3-D irradiance to be ray-traced we used hourly averaged irradiation data from STRANG (STRANG, 2009). A few days during spring time for the location Utrecht, The Netherlands, were used as input.

The second CAD scenery has been modeled according to the involved geometries where a PV powered mouse (Reich et al., 2009) was measured, illustrated in Fig. 4. As shown, several 3-D geometries are accounted for in high detail. The short circuit current output of the cell incorporated in the mouse was obtained by measuring the voltage drop over a measurement shunt, as was the short circuit current of a reference cell located outside the building

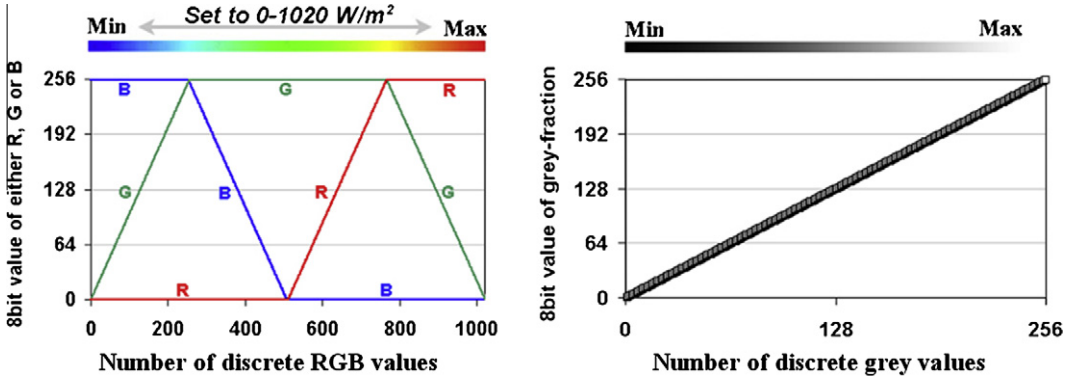

Fig. 1. RGB- and grey-scales compared for the case of 8 bit data values. For Eq. (1), normalized values are referred to (range 0–1 instead of 0–256). The four intervals concerned are marked by increasing 'G', decreasing 'B', increasing 'R' and decreasing 'G'. In the first interval, only 'G' increases. By stating 'G' in the equation, the scale will thus range from 0–1. In the second interval, B decreases, thus mirroring 'B' is necessary. As B starts at one, additionally accounting for the offset gives '$-(B-1)$', which is simplified to '$1-B$'. The second interval then ranges from 1–2, as G remains 'one'. Further, as 'B' remains zero throughout intervals 3 and 4, the 'one' of 'B' is added continuously (as '$1-B=1$' results). It thus follows $R(3-2G)$ for a continuous scale in intervals 3 (increasing R, $G=1$) and 4 (decreasing G, $R=1$).

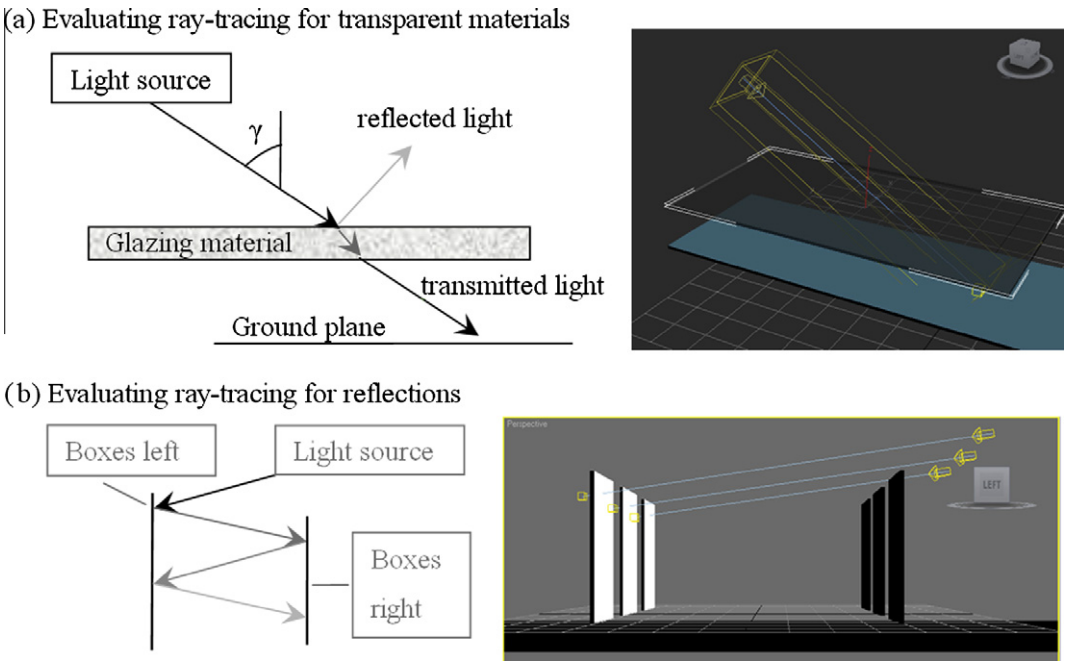

Fig. 2. Validation of ray-tracing accuracy for: (a) transmitted light and (b) reflected light, illustrated in schematic drawings (left) and screenshots of the corresponding scenery (right). The shown boxes are planar, also 2-D planes could have been used.

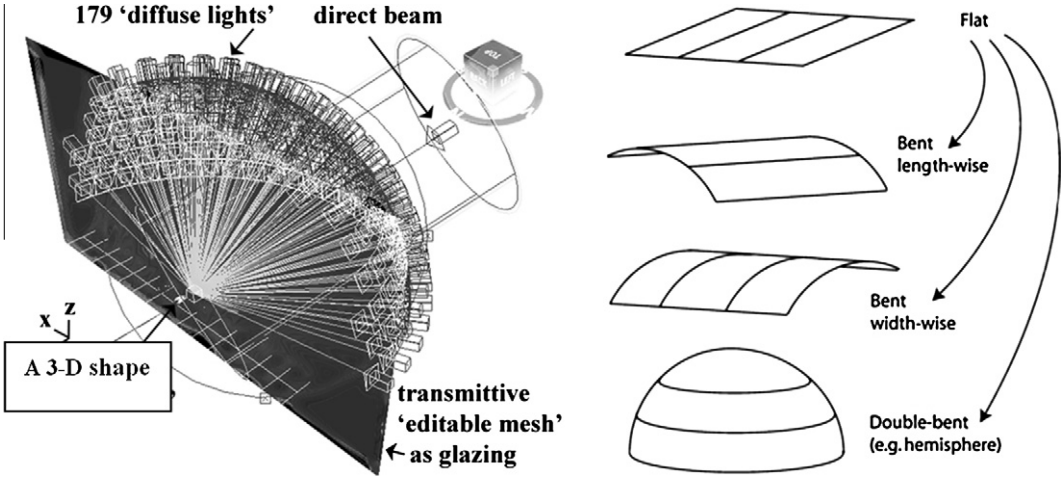

Fig. 3. The simplified CAD scenery of a window sill (left) and 3-D shapes used in the simulations (right).

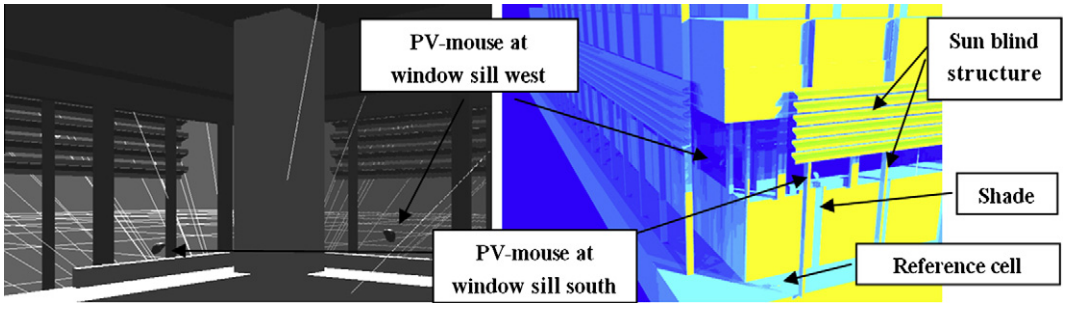

Fig. 4. The 3-D modeled CAD scenery in which the PV output of the mouse was also measured, viewed from indoors (left) and RGB encoded viewed from outdoors (right).

(see Fig. 4, right). Data was measured at 1-s resolution and averaged over 15 s.

2.5. Modeling PV power output

Irradiance intensity dependent cell efficiency, measured at the maximum power point, depends strongly on the particular PV type and cell quality that influences shunt resistance and the diode current (Reich et al., 2009). As a result, logarithmically decreasing PV efficiency towards lower intensity leads to disproportionally lower PV power output in low light situations. However, detailed PV modeling requirements are beyond the scope of this paper. To this end, the PV power output and energy yield is determined by the equation introduced in Reich et al. (2009) that parameterizes solar cell efficiency (η) as a function of irradiance intensity in the maximum power point using four parameters:

$$\eta(I) = a_1 + a_2 I + a_3 \ln(I + a_4) \quad (3)$$

We presented attainable accuracies to model PV performance as a function of irradiance intensity for crystalline silicon cells (Reich et al., 2009; Alsema et al., 2005), earlier work by Randall (2003), Randall et al. (2001) and Gemmer, 2001 dealt with many different PV types. Any further effects are omitted, amongst which for example spectral effects, operating temperatures different from STC, operating voltages different from the maximum power point, and charge efficiencies of charge electronics involved in the PV mouse.

3. Results

3.1. Theoretical validation

The expected- and CAD simulated light intensities were found to be in excellent agreement for all cases: (1) incident angle resolved transmission of light); (2) reflected light (Fig. 6) and (3) super-position of 3-D irradiance simulated in CAD (Fig. 7). Each case is described in detail hereunder.

First, ray-tracing accuracy with respect to light transmittance through (transparent) materials was evaluated. Simulated intensity as a function of incident angle is shown in the left panel of Fig. 5. The amount of light transmitted through a material compared to the amount of light in the absence of that material represents the transmittance fraction, shown in the right panel of Fig. 5. Simulated transmission fractions (circles) match those modeled by Fresnel equations (lines) very well. Only small scattering due to numerical errors can be observed. To obtain excellent agreement of simulated to expected intensities, however, it emerged that settings in the graphical user interface (GUI)

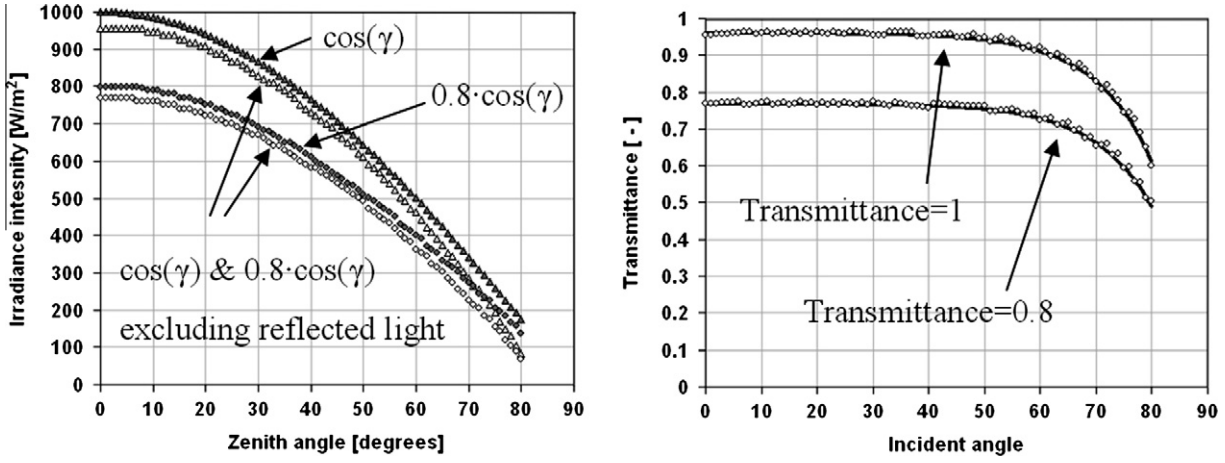

Fig. 5. Theoretical validation of ray-tracing accuracy for light transmission as a function of incident angle. Absolute intensity values (shown left) are used to calculate transmission fractions (shown right).

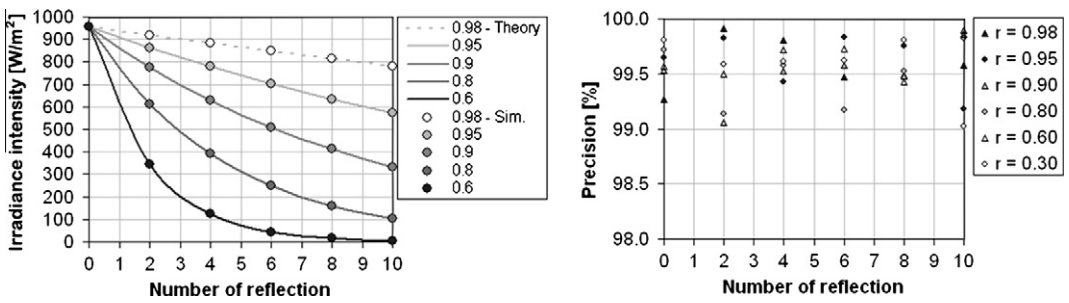

Fig. 6. Theoretical validation of ray-tracing accuracy for reflected light as a function of involved reflections.

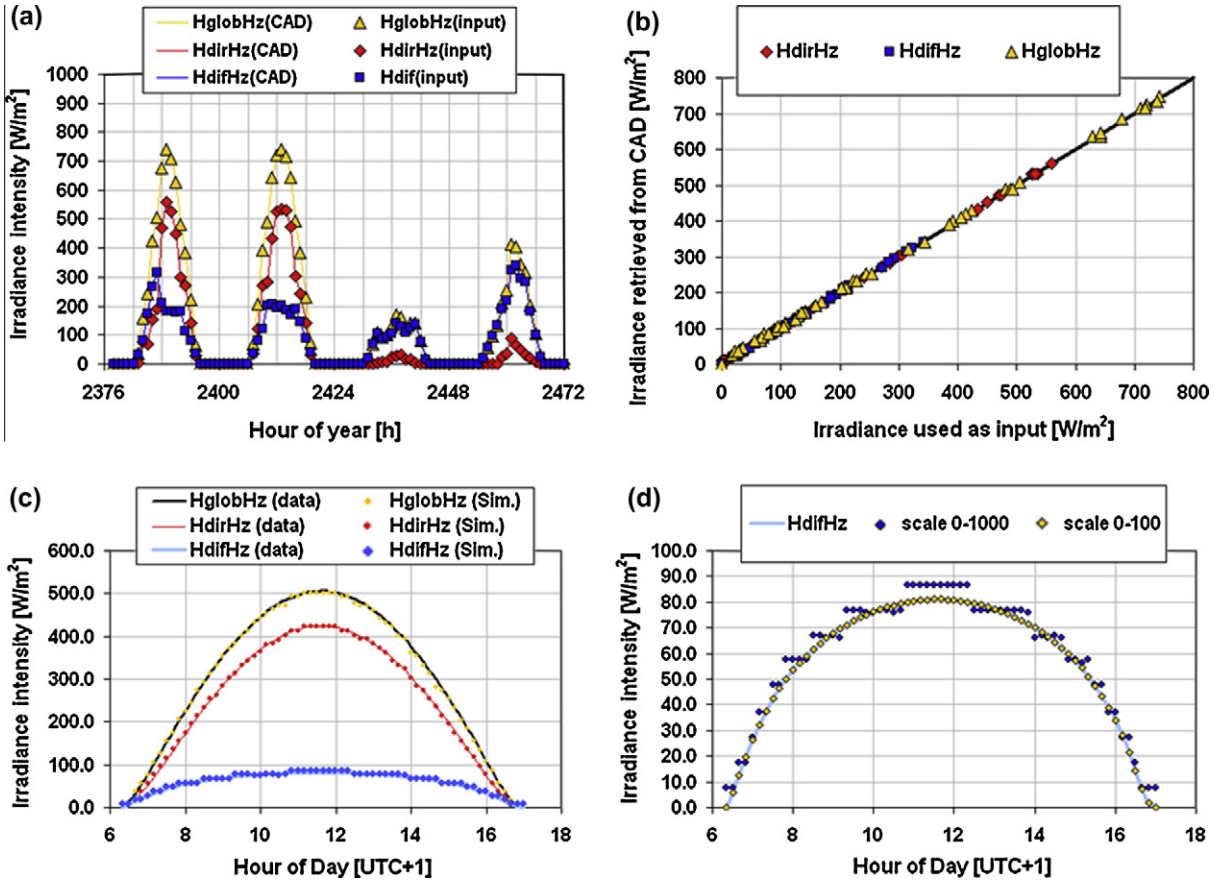

Fig. 7. Horizontal (HZ) intensities used as input compared to the CAD simulated horizontal intensities for direct (dir) diffuse (dif) fractions as well as global (glob) intensity.

of the 3ds Max software must be chosen carefully. Here, the range indicated between 0 and 1 in the GUI of 3ds Max does not represent the reflectivity of a surface in physical terms, whereas transparency is expressed in a conventional way (with a range of 0–1 indicating transmittance). The value to be entered as 'reflectivity' in 3ds Max ('material-property' GUI) only expresses to which extent reflections are accounted for. Setting this parameter to 0.5 would not achieve 50% reflectivity, but only half of the reflections based upon IOR and Fresnel algorithms would be obtained. The case shown in Fig. 5 is the pre-defined (mi)-material 'solid glass' (IOR = 1.52).

To simulate reflections, only one of the parallel planes was considered here (see Section 2), therefore only intensities associated to every second reflection are shown. Light was incident onto an area of ~20 × 20 pixels so that each intensity data point refers to ~400 RGB intensity values. As expected, the precision with which reflections can be ray-traced is very high (Fig. 6).

The 3-D distribution of irradiance simulated in the 3-D scenery of 3ds Max was validated next. To this end, the input data of irradiances was compared to intensities obtained from ray-traced, rendered and RGB converted data for each irradiance fraction individually (direct-beam, diffuse and global horizontal). A horizontal plane was therefore simulated with a number of light sources arranged as a hemisphere in the CAD environment. Again, very good agreement is found, which also proves the superposition of irradiance intensity holds when using multiple light sources (Fig. 7). The time course data shown here was also used in the following simulations. The STRANG data series was used for simulating the 3-D shapes as well as the PV powered mouse (results presented in Sections 3.2 and 3.3). The STRANG web-service provides hourly averages of direct-beam and global horizontal intensities "*for the geographic area of Scandinavia and the run off region of the Baltic sea*" (STRANG, 2009). The Bird model (Bird et al., 1981) was used as a basis to compare simulated PV output of the mouse with measured data (results presented in Section 3.4). This model calculates clear-sky irradiance intensities for a fixed set of atmospheric conditions, for which we kept the default values.

Some minor deviations between the input data (the intensities of STRANG and Bird models used as input) and the CAD simulated and RGB converted intensities, however, do occur. These (numerical) inaccuracies are illustrated for the diffuse fraction of the clear-sky data in Fig. 7d. Whereas the RGB scale of ~0–1000 W/m^2 results in a numerical resolution of ~8 W/m^2, adapting the scale to 0–100 W/m^2 alleviates these numerical inaccuracies (as

the resolution is then ~0.8 W/m^2). With the number of discrete RGB values being precisely 1020 and the scale also set to precisely 0–1020 W/m^2 (see Section 2), one would expect 1 W/m^2 as the numerical resolution. The numerical resolution of the 3ds Max rendering process therefore seems to be limited to 128 values under considered settings (1000 W/m^2 range divided by the resulting resolution of 8 W/m^2).

3.2. Irradiation intensity distributions incident onto 3D-geometries

The rendered bitmap images of the 3-D shapes describe a 2-D distribution of irradiance incident onto a surface. Hence, the 3-D perspective is lost. From within the 3ds Max graphical user interface, however, it is possible to render geometries in 3-D (Fig. 8a). Here, rendered irradiance distributions occurring at a summer day at solar noon are shown. For a single bend shape, irradiance is distributed unequally perpendicular to the bend (Fig. 8b). Unequal distributions in only the width-wise direction are useful, as only part of the entire surface length must be considered, e.g. Fig. 8c.

The bending radii of single bend geometries have been set to 60°, 120° and 180°, whilst a hemisphere is used as a double-bend surface. Furthermore, different orientations of the single bend geometries are considered, by orientating the bending axis of the shapes either parallel or perpendicular to the south-facing window. The irradiance distributions during the 4 days considered (see STRANG data, Fig. 7) of overall six distinct geometries are shown together with daily aggregated irradiation (hemisphere) in Fig. 9.

The resulting distributions of incident irradiance onto the particular shapes show that CAD rendering can be very helpful to visualize irradiation patters. This data in graphical form may already help in the development or design of PV systems, by visualizing irradiance distributions that are beyond intuition otherwise. In particular, the aggregated irradiation incident onto the hemisphere can be very helpful in that it assesses the amounts of irradiances incident from multiple directions.

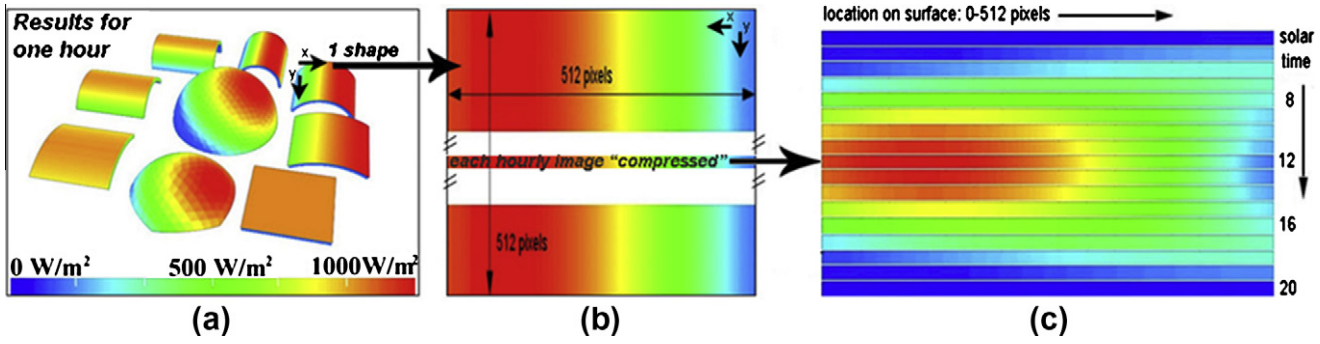

Fig. 8. Rendered irradiance intensity distributions for 3-D shapes: (a) viewed form within the 3ds Max GUI; (b) illustrating a 'compressed' way of showing obtained irradiation distribution data, which allows to; (c) present intensity distributions incident onto a single-bent surface during the course of an entire day, in a single image.

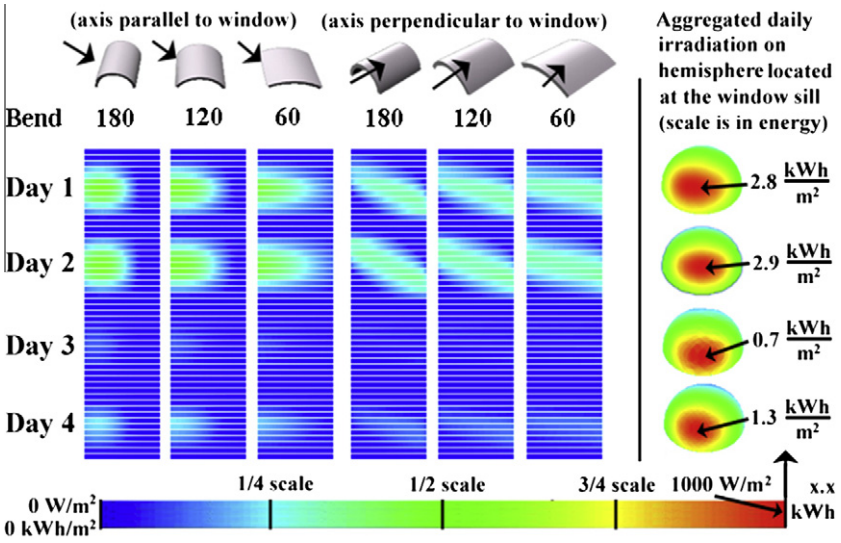

Fig. 9. Rendered irradiance intensity distributions for all 3-D shapes.

3.3. Image processing to simulate interconnected PV cells

The same STRANG irradiation data simulated for the 3-D shapes was now used to simulate intensity distributions incident onto the solar cell surface of the PV mouse. Simply averaging irradiance incident onto the entire cell area could be used to model the PV output. To also account for series-interconnected cells, however, rendered RGB-images of the PV area (step 1) can be assumed to consist of a number of series-interconnected cells (step 2), illustrated in Fig. 10. Assuming a number of cells allows to average irradiance intensity incident onto each cell individually (step 3), in turn allowing to account for the least illuminated cell in PV output calculations (step 4), which gives different (lower) values compared to averaging irradiance over the entire cell area (denoted (5) in Fig. 10). This example only illustrates one possible way on processing gathered irradiance distributions. In case of the mouse, only a single cell is incorporated.

3.4. Simulated and measured PV output of the 'SoleMio' PV mouse

To show that high accuracies of the presented 'CAD-PV' simulation approach can be obtained also in practice, we focused on 4 days in the measurement period during which substantial amounts of direct-beam intensities happened to prevail. Large amounts of direct-beam intensities are focused, because the resulting pattern is visualized better compared to highly scattered data (intermediate and overcast skies only). Also in the 4 day period, however, substantial cloud cover implies lowered intensities compared to the clear-sky case. This is illustrated in Fig. 11, which depicts the simulated data for the case of only clear-sky conditions and all measured data. As shown, the shading pattern (caused by objects depicted in Fig 4) is modeled very accurately. With only the clear-sky case simulated, however, measured PV output is overestimated when cloud cover lowers the PV power output considerably.

In another simulation of the 4 days we therefore also took into account that direct-beam intensities are reduced substantially under cloudy skies, whereas the diffuse component of solar energy slightly increases in this case. The original clearness index (k_t) equation of Orgill and Hollands, (1977) are used to determine direct/diffuse fractions. It proved necessary to scale measured global horizontal intensity with a factor (1.4) to obtain plausible direct/diffuse fractions. This aberrance is due to the shade thrown onto the reference cell by the building (see Fig. 4) and the glass cover of the reference cell that reflects light particularly at large incident angles. The direct and diffuse horizontal intensities, together with calculated k_t, are shown in Fig. 12. In addition, the irradiance measured by the (horizontal) reference cell and the theoretical clear-sky global horizontal intensity are included. Only the first day of the measurement period is shown (Fig. 12, left). In addition, 1 h within this day is shown to illustrate variations of irradiance and thereto associated sky conditions within one

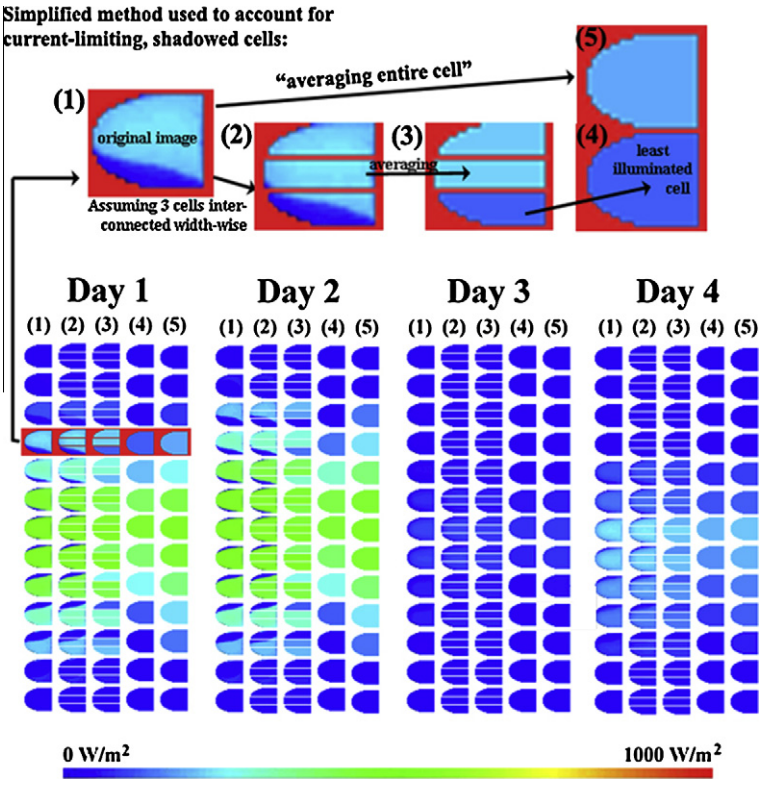

Fig. 10. Accounting for series-interconnected cells in a simplified method.

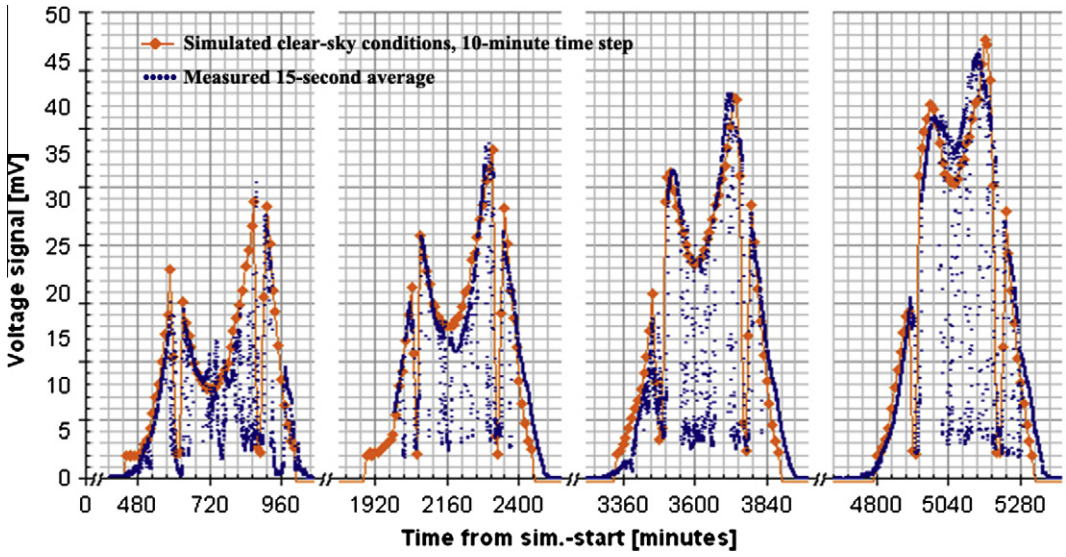

Fig. 11. Measured 15-s data of PV-output (voltage signal of measurement shunt) compared to 10-minutely simulated PV-output. For the simulation, clear-sky conditions were simulated as the 3-D irradiation in CAD. As a result, the simulated data corresponds to only the highest measured data values.

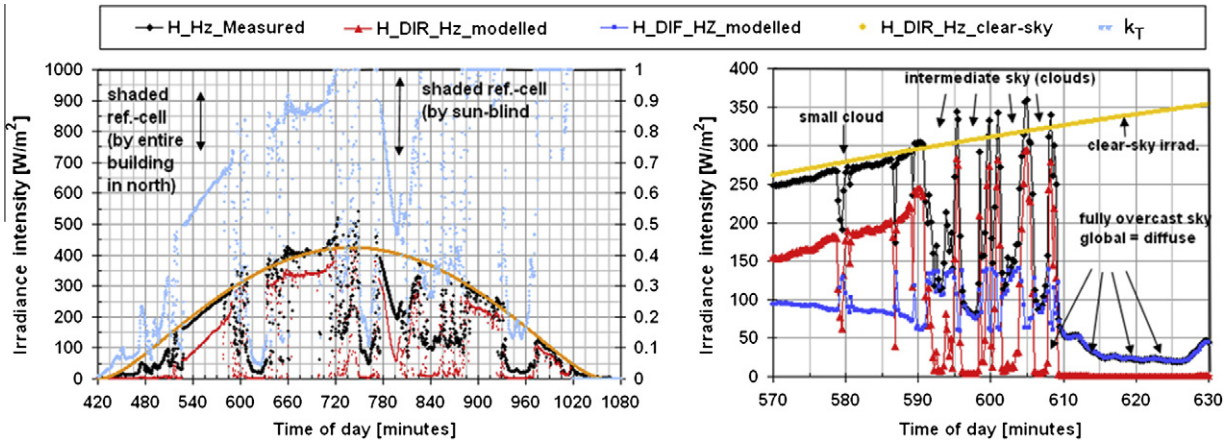

Fig. 12. Modeled instantaneous direct and diffuse irradiance fractions. These irradiance fractions are the input to model solid-angle distributions using the Perez model, which are in turn modeled as 3-D irradiance in CAD software.

single hour (Fig 12, right). In the first 20 min of this hour, measured intensities show that clear-sky conditions prevailed, followed by intermediate sky conditions for another 20 min. Here, direct-beam intensity is modeled to be much lower (or zero) when the sun is covered by a passing cloud. In this case, diffuse fractions slightly increase. In between passing clouds, additional direct-beam sunlight that is reflected by clouds is incident onto the horizontal surface as well, explaining slightly higher intensities measured in between passing clouds. In the last 20 min of this hour fully overcast conditions lead to direct-beam intensities being zero.

The CAD ray-tracing simulations were then performed for: (1) the entire four day duration with 10-min averaged data; and (2) for the 1 h shown in Fig. 12, using the original 15-s data. In both cases, very good agreement of simulated and measured data is obtained, illustrated in Fig. 13. The scattering of measured compared to simulated data in the entire measurement period of the 4 days is reduced for hourly averaging the 10-min simulated data already (Fig 13, left). Although deviations of ~20% can be observed for intermediate sky conditions, also the simulation results of instantaneous data are in very good agreement to measured data. Overall only small offsets and minor deviations can be discerned for simulated compared to measured 15-s irradiation data (Fig. 13, right).

Finally, the PV output was modeled. Three cells with different weak-light performances have been considered. Efficiencies corresponding to modeled weak-light performances are illustrated in Fig. 14 (left). The parameters $a1$–$a4$ with which the intensity dependent efficiencies have been calculated are included in Table 1, which also lists the simulated PV yields. Simulated PV yields will be almost equal to those measured, as can be concluded from the histogram plots of both simulated and measured intensities, which are almost identical, see Fig. 14 (right).

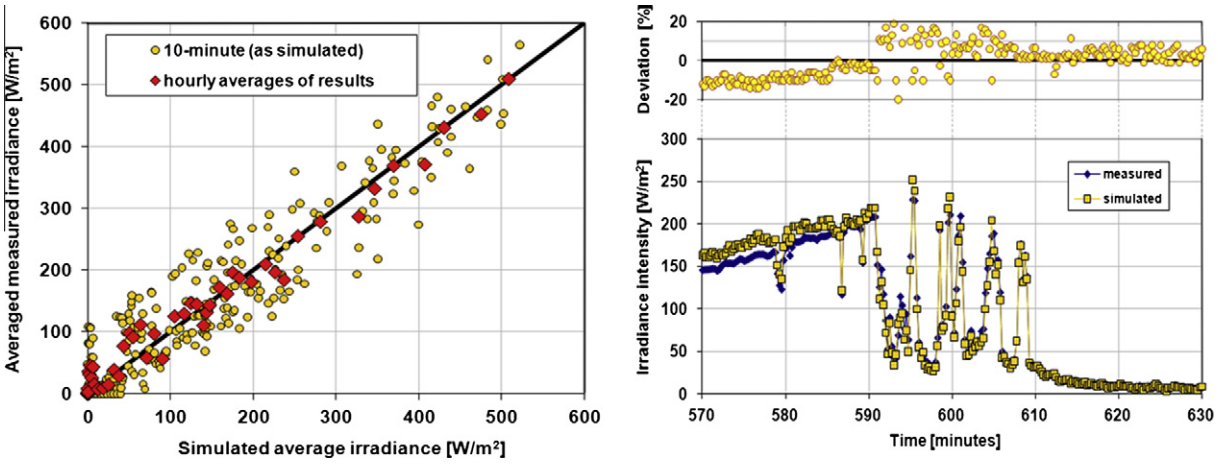

Fig. 13. Simulated compared to measured irradiance intensity averaged over the entire PV are incorporated into the PV mouse. The entire period using 10-min time steps is shown in the left panel. Instantaneous irradiance intensities and the %-deviation of simulated compared to measured data are shown in the right panel.

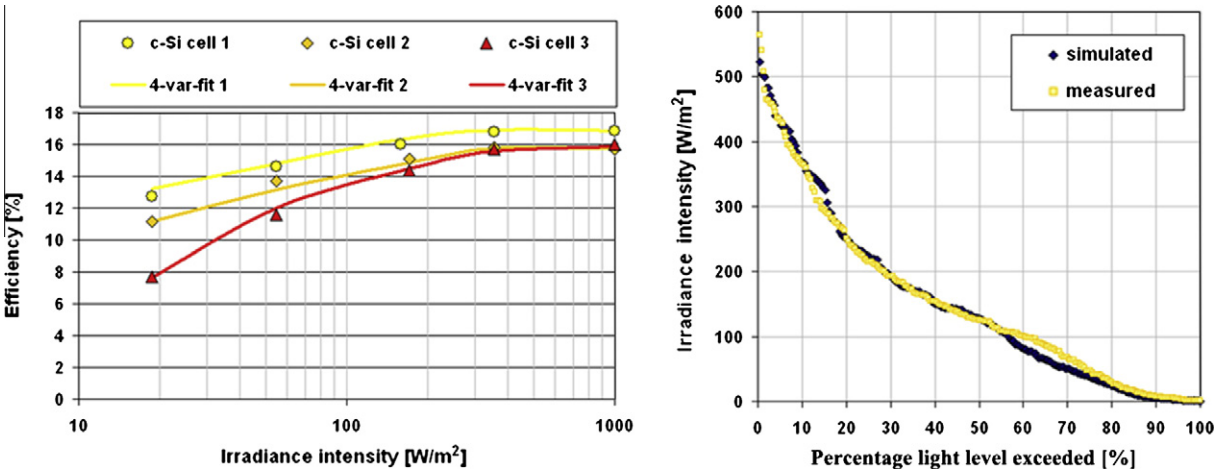

Fig. 14. Almost equal frequency distribution of measured and simulated intensity as well as weak-light performance of selected crystalline silicon solar cells.

Table 1
Charge yield during the simulated 4 days period for the SoleMio PV-mouse, see text.

Cell number	Parameters of solar cell conversion efficiency, see Eq. (2)				Simulated energy yield 'SoleMio' (totals calculated for entire 4 days using simulated irradiation intensities and Eq. (2), Wh)
	$a1$	$a2$	$a3$	$a4$	
1	9	−0.0025	1.5	2	287
2	6	−0.003	1.85	1	265
3	4.4	−0.003	2.1	0	260

4. Discussion

We presented a PV energy yield simulation approach with which virtually any three-dimensional (3-D) scenery and irradiance condition can be modeled and that in terms of accuracy gives excellent results. Compared to (commercially) available PV simulation software, this is an important improvement, and therefore of value to not just the Product Integrated PV (PIPV) field. One promising application of 'CAD–PV' simulations would be, for example, Building Integrated PV (BIPV). Architects and product designers already extensively use CAD programs and renderings in their daily work-routine. However, also concerning sun-tracking and concentrating systems it is an interesting concept. Due to the versatility of CAD software, not only specific 3-D geometries of particular tracking- or concentrator systems could be modeled but also their moving or rotating elements could be included (the creation of animations is another standard feature of many CAD programs). Also in case of free standing, open-space PV systems 'CAD-PV' simulations could be helpful. Here, complex 3-D terrains or self-shading of sun-tracked PV-module areas could be modeled, both of which is very difficult to achieve with currently available software.

One main drawback of the approach, however, is the relatively large computational effort. Dependent on the rendered scenery and the number of light sources, several

minutes may be required to render a single image. Rendering speed could be increased by reducing (1) the number of pixels to be rendered, (2) the number of light sources to model solid-angle irradiance distributions and (3) the 'tracing-depth' of reflections to be ray-traced. Also increasing the computational power can decrease simulation durations. Last but not least, a de-coupling of the CAD ray-tracing from the processing of time course data could be realized. Here, ray-tracing individual sky zones could determine Irradiance Distribution Matrices representing 2-D distributed light intensity incident onto the PV area. Such matrices related to each sky zone individually would need to be ray-traced only once, thus avoiding the ray-tracing of light originating from equal directions in the sky for a number of times.

Not included in this study were spectral- (Gueymard, 2009) and polarization-effects of light (Krauter and Hanitsch, 1996). However, wavelength-resolved transmission characteristics of transparent geometries or wavelength-resolved albedo coefficients of reflecting geometries can have a decisive influence, particularly for the window sill case focused in this study. Glazing coatings act as spectrally selective filters and are frequently incorporated into nowadays windows, leading to large differences of PV power output for different window types. We recently reported that the decrease of the short circuit current density for crystalline silicon based cells can deviate up to 13%, only due to spectral effects introduced by window glazing (Reich et al., 2009). Here, a spectral mismatch factor (MMF) may account for spectral effects. To this end, the current output of PV in the reference case (here short circuit current density at Air Mass (AM) 1.5, denoted $J_{SC,AM1.5}$) and the spectral composition $E(\lambda)$ of available light together with the PV Spectral Response $SR(\lambda)$ of the specific cell concerned would need to be combined:

$$\mathrm{MMF} = \frac{J_{SC,AM1.5}}{\int_{\lambda} E(\lambda) \cdot SR(\lambda) \cdot d\lambda} \tag{4}$$

Another, very practical problem of the simulation approach is related to the irradiation data that can be used as input for the simulation. This problem is shared with most other solar energy simulation approaches, because on-site data is most often not available or is of low quality (meaning data includes either errors or, for example, does not provide differentiated direct-beam and diffuse fractions, etc.). As a result, satellite-imagery derived irradiation series modeled to be incident at the earth' surface have enjoyed increased popularity, because this data is available for virtually any location. The error in such data, however, can be very high. Here, for demonstration purposes we used irradiation series obtained from the STRANG service (STRANG, 2009). "*The error when comparing hourly model data with point observations is approximately 30% for the global and the CIE UV irradiance while it is about 60% for the direct irradiance and the sunshine duration.*" (STRANG, 2009). Such inaccuracies in irradiation data make comparisons of measured to simulated data pointless, if considering only a few days. Here, future research is needed to evaluate accuracies that can be obtained for longer measurement durations. With the presented simulation concept capable of accounting for complex shading patterns, this may also include the question with which averaging duration solar energy distributions need to be simulated, particularly if (severe) shading is involved.

As of yet no Graphical User Interfaces (GUIs) are available, making it rather inconvenient and difficult to use CAD programs for PV yield predictions. However, the development of sophisticated 3-D drawing software (and GUIs) as well as ray-tracing and rendering software is not required, because the presented concept only exploits these features of readily available software. Theoretically, any rendering program can be used, which may greatly facilitate the practical utilization and further development of this concept.

5. Conclusions

We presented a simulation concept for PV energy yield predictions that makes use of three-dimensional (3-D) drawing, ray-tracing and rendering features of CAD software. To ensure accurate simulation results are obtained, the solar irradiation data used as input is compared to irradiation data derived from rendered images, proving high accuracy of 3-D irradiance simulations in 3-D CAD sceneries. As expected, also ray-tracing precision (light transmission and reflection) proves to be very high in CAD. It is then demonstrated that simulated PV yields of a Product Integrated PV (PIPV) system agree very well with those measured. Overall, the simulation concept is a very promising one. Simulating irradiation distributions also for complex, three-dimensional (3-D) shapes under complex (3-D) irradiation is possible straightforwardly. The utility of this tool is thus not just of value to the PIPV field but can be of use for e.g. Building Integrated PV (BIPV) or sun-tracking and concentrator systems as well.

Acknowledgements

This work was financially supported by the NWO-SenterNovem Energy Research programme through the SYN-Energy project (Alsema et al., 2005). We would like to acknowledge textual suggestions of and fruitful discussions with Angele Reinders and Hugo de Wit from the University of Twente during the preparation of this work.

References

Alsema, E.A., Elzen, B., Reich, N.H., Van Sark, W.G.J.H.M., Kan, S.Y., Silvester, S., Veefkind, M., Jelsma, J., 2005. Towards an optimized design method for PV-powered consumer and professional applications – the syn-energy project. In: Hoffmann, W., Bal, J.-L., Ossenbrink, H., Palz, W., Helm, P., (Eds.), Proceedings of 20th European Photovoltaic Solar Energy Conference. Barcelona, Spain: WIP, Munich, Germany, pp. 1981–1984.

Bird, R.E., Hulstrom, R.L., 1981. Simplified Clear Sky Model for Direct and Diffuse Insolation on Horizontal Surfaces, Report Technical Report No. SERI/TR-642-761, Solar Energy Research Institute.

Gemmer, C., Schubert, M.B., 2001. Solar cell performance under different illumination conditions. In: Proceedings of Material Research Society Symposium, pp. A25.29.21–A25.29.26.

Grena, R., 2008. An algorithm for the computation of the solar position. Solar Energy 82 (5), 462–470.

Gueymard, C.A., 2009. Daily spectral effects on concentrating PV solar cells as affected by realistic aerosol optical depth and other atmospheric conditions. In: Proceedings of Optical Modeling and Measurements for Solar Energy Systems III, San Diego, CA, USA: SPIE, pp. 741007–741014.

Kovach, A. 1994. Effects of inhomogeneous irradiation distribution on a PV array inan urban environment. In: Proceedings of Twenty Fourth IEEE Photovoltaic Specialists Conference, Waikoloa, HI, USA, pp. 994–997.

Krauter, S., Hanitsch, R., 1996. Actual optical and thermal performance of PV-modules. Solar Energy Materials and Solar Cells 41–42, 557–574.

Larson, G.W., Shakespeare, R. 1998. Rendering with Radiance. Morgan Kaufmann.

Murdock, K.L., 2008. 3ds Max 2009 Bible. Wiley.

Nieuwenhout, F., van der Borg, N., van Sark, W.G.J.H.M., Turkenburg, W.C., 2007. A new method for estimating insolation based on PV-module currents in a cluster of stand-alone solar systems. Progress in Photovoltaics: Research and Applications 15 (5), 387–404.

Orgill, J.F., Hollands, K.G.T., 1977. Correlation equation for hourly diffuse radiation on a horizontal surface. Solar Energy 19 (4), 357–359.

Perez, R., Seals, R., Ineichen, P., Stewart, R., Menicucci, D., 1987. A new simplified version of the perez diffuse irradiance model for tilted surfaces. Solar Energy 39 (3), 221–231.

Randall, J.F., 2003. On the Use of Photovoltaic Ambient Energy Sources for Powering Indoor Electronic Devices. Thesis, Ecole Polytechnique Fédérale de Lausanne.

Randall, J.F., Droz, C., Goetz, M., Shah, A., Jacot, J., 2001.Comparison of 6 photovoltaic materials across 4 orders of magnitude of intensity. In: McNelis, B., Palz, W., Ossenbrink, H., Helm, P., (Eds.), Proceedings of 17th European Photovoltaic Solar Energy Conference. Munich, Germany: WIP-Renewable Energies, Munich, Germany, pp. 603–606.

Reich, N.H. 2006. A PV powered computer mouse as case study for PV powered consumer systems. In: Poortmans, J., Ossenbrink, H., Dunlop, E., Helm, P., (Eds.), Proceedings of 21st European Photovoltaic Solar Energy Conference and Exhibition, Dresden, Germany: WIP-Renewable Energies, Munich, Germany, pp. 2306–2311.

Reich, N.H., Van Sark, W.G.J.H.M., Alsema, E.A., Reinders, A.H.M.E., de Wit, H., 2008. A CAD based simulation tool to estimate energy balances of device integrated PV systems under indoor irradiation conditions. In: Proceedings of 23rd European Photovoltaic Solar Energy Conference, Valencia, Spain, pp. 3338–3344.

Reich, N.H., Van Sark, W.G.J.H.M., Alsema, E.A., Lof, R.W., Schropp, R.E.I., Sinke, W.C., Turkenburg, W.C., 2009. Crystalline silicon cell performance at low light intensities. Solar Energy Materials and Solar Cells 93 (9), 1471–1481.

Reich, N.H., Veefkind, M., Sark, W.G.J.H.M.v., Alsema, E.A., Turkenburg, W.C., Silvester, S., 2009. A solar powered wireless computer mouse: industrial design concepts. Solar Energy 83 (2), 202–210.

Reich, N.H., Van Sark, W.G.J.H.M., Reinders, A.H.M.E., de Wit, H., 2009. Using CAD software to simulate PV energy yield: predicting the charge yield of solar cells incorporated into a PV powered consumer product under 3-D irradiation conditions. In: Proceedings of Photovoltaic Specialists Conference (PVSC), IEEE, Philadelphia, pp. 1291–1296.

Reich, N.H., Van Sark, W.G.J.H.M., Alsema, E.A., Netten, M.P., Silvester, S., 2007. Practical experiences with the "Sole-Mio" solar powered computer mouse. In: Proceedings of 22nd European Photovoltaic Solar Energy Conference, Valencia, Spain, pp. 3121–3125.

Reinders, A.H.M.E., 2007. A design method to assess the accessibility of light on PV cells in an arbitrary geometry by means of ambient occlusion. In: Proceedings of 22nd European Photovoltaic Solar Energy Conference, Milan, Italy.

Roth, W., 2008. 40 Jahre Photovoltaik-Geräte-Entwicklung in Deutschland. In: Proceedings of Symposium Photovoltaische Solarenergie, Bad Staffelstein, pp. 110–116.

STRANG, 2009. Swedish Meteorological and Hydrological Institute (SMHI). <http://produkter.smhi.se/strang/>.

Wagemann, H.G., Estrich, H., 1994. Grundlagen der photovoltaischen Energiewandlung. Stuttgart Teubner, Germany.